*Journal of Network Intelligence*
**Taiwan Ubiquitous Information**
 ISSN 2414-8105
Volume **9**, Number **1**, February **2024**

# Vegetation Resource Classification on Deep Neural Network and Composite Remote Sensing Image Data

Wei Sun*

School of Architectural Engineering
Tongling University
Tongling 244000, P. R. China

College of Forestry
Beijing Forestry University
Beijing 100083, P. R. China
vvsmilesunwei@126.com

Yao-Cheng Su

812 Geological Team
East-China Metallurgical Bureau of Geology and Exploration
Tongling 244000, P. R. China
syc18005625741@163.com

Ying Zhang

College of Natural Resources and Environment
South China Agricultural University
Guangzhou 510642, P. R. China

Tangshan Vocational and Technical College
Tangshan 063000, P. R. China
zhangying529@163.com

Viktor Gruev

School of Education
Grenfell Campus, Memorial University of Newfoundland
Corner Brook A2H 5G4, Canada
bh9825@163.com

*Corresponding author: Wei Sun
Received August 29, 2023, revised October 21, 2023, accepted December 7, 2023.

Abstract. *The classification of vegetation resources based on remote sensing images can provide important data support for forest resources survey, grassland monitoring, and wetland vegetation change monitoring. Remote sensing images can quickly and widely obtain the distribution of vegetation resources and its change information, combined with classification algorithms can achieve the extraction of vegetation type and coverage, which provides an effective means for the relevant departments to carry out the survey and monitoring of vegetation resources, and greatly improves the work efficiency. Deep learning methods show high performance as big data mining tools. However, when dealing with remote sensing image tasks, such as the vegetation resource classification problem, it exhibits low accuracy and efficiency. Therefore, a vegetation resource classification method based on deep neural networks and composite remote sensing image data is proposed. Firstly, composite Remote Sensing (RS) image data based on Geographic Information System (GIS) is used to extract relevant attribute data and spatial data of vegetation resources to form a preliminary input image. Following the extraction of several local characteristics from the initial input picture, the deep neural network employed for judgment is fed with these features. The assigned picture labels are used to categorize each local feature. The overall image is adjudicated based on a simple voting method. Finally, classification experiments are conducted using WorldView2 high resolution satellite remote sensing image data, which shows that the proposed method outperforms other classification methods and has better classification accuracy and classification efficiency.*
**Keywords:**Remote sensing imagery; GIS; Local classifiers; Deep learning; Deep neural networks

1. **Introduction.** Remote sensing satellites are artificial satellites that allow remote sensing in outer space and continuous observation of the corresponding areas of the earth's surface on demand. Currently, remote sensing technology is widely used in various fields. Remote sensing data acquired by various sensors can be converted into visible images by simulating human visual system techniques [1,2].

The classification of vegetation resources in remote sensing images can provide important data support for forest resources survey [3], grassland monitoring [4], and wetland vegetation change monitoring [5,6]. Remote sensing images can quickly and widely obtain the distribution of vegetation resources and its change information, combined with classification algorithms can achieve the extraction of vegetation type and coverage, which provides an effective means for the relevant departments to carry out the investigation and monitoring of vegetation resources, and greatly improves the efficiency of the work [7]. The results of remote sensing vegetation classification can also be used for agricultural applications such as vegetation species identification, crop yield estimation, and ecosystem service assessment [8,9]. In general, remote sensing vegetation classification is one of the key techniques to achieve quantitative survey [10] and dynamic monitoring of vegetation resources.

Fabbrocino et al. [11] proposed a spatial database and management system of hydrological ecology based on Geographic Information System (GIS), which realised standardised and visualised spatial information storage and management, and enhanced the efficiency of vegetation resources research. However, there is a problem of poor accuracy in the way of using only a single technical means of GIS. In recent years, Remote Sensing (RS) technology combined with GIS technology has played an important role in green environmental protection, Garouani et al. [12] carried out an in-depth study on the evolution of vegetation cover and surface temperature based on RS and GIS, and used several remote sensing images in the ENVI5.0 software [13] for the inversion of the calculation, which provides data support for environmental protection. environmental protection.

RS-based image classification is a very important task in computer vision tasks because many practical social application scenarios require correct image classification results, such as visual surveillance, marketing, object tracking, big data analysis, and so on. Image classification, like other classification problems, is generally divided into several steps [14,15]: target detection, image preprocessing, feature extraction and classification. Most of the traditional high-resolution remote sensing image classification uses object-oriented classification methods. In the detection stage, Patch sections in the picture are found and separated. Following that, preprocessing methods are employed to minimize disparities in size and lighting, and the patch objects are used as basic units to achieve classification. However, object-oriented classification methods have too many classification attributes, which results in generally low classification accuracy.

Deep neural networks have shown their excellent performance in computer vision tasks. However, using standard deep neural networks to learn directly from the whole image is sometimes very difficult, especially for complex data such as natural images. Extracting information based on subregions of the original image can effectively solve this problem. For example, unsupervised learning extracts useful features from image units [16], which are called image blocks.

Therefore, the objective of this study is to develop an automated, generalised and highly accurate vegetation classification technique using deep neural networks and composite remote sensing (RS) image data, in order to provide better technical means for vegetation resource investigation and monitoring.

1.1. **Related Work.** It is well known that feature extraction is a crucial step to achieve good performance. Learning algorithms have become a very popular area of research because they enable algorithms to automatically find the best representation of the data [17, 18].

Deep neural networks can extract high-level semantic features from remote sensing images and identify different types of vegetation more accurately than traditional methods. Deep learning technology can achieve end-to-end automatic classification without manual extraction of features, and automatically monitor the distribution of vegetation resources and its dynamic changes. The use of deep learning techniques to classify remote sensing vegetation resources has become a hot direction in related fields. For example, Wang et al. [19] trained a convolutional neural network model using UAV remote sensing images with the idea of transfer learning to achieve the extraction of rice planting areas, and the average classification accuracy reached 94%, and Zhou et al. [20] trained a deep learning model to achieve the classification of vegetation by using the multi-temporal phase data from Sentinel-2 satellite. Zhou et al. [20] used Sentinel-2 satellite multi-temporal data to train a deep learning model to achieve vegetation classification, and the results show that the deep learning method can significantly improve the classification accuracy. Zhao et al. [21] constructed an integrated convolutional neural network and recurrent neural network to achieve the classification of vegetation time series based on hyperspectral data, and the classification effect is better than that of a single model. Guo and Ren [22] demonstrated that the composite remote sensing images of different temporal phases and different wavelength bands can provide richer features, which is conducive to improving the classification accuracy. features, which is conducive to improving the classification accuracy. By constructing a more complex deep neural network model and optimising it with a large amount of training data, a better generalisation ability can be obtained, which can be adapted to the classification of vegetation types in different areas.

1.2. **Motivation and contribution.** Through the above analysis, it can be seen that the current deep learning technology has been widely used in remote sensing vegetation

classification tasks. By constructing models such as deep convolutional neural network (DCNN) [23] and deep recurrent neural network (DRNN) [24], the high-level features of the remotely sensed images can be extracted effectively to achieve the accurate classification and identification of vegetation resources. However, only using deep learning techniques to achieve remote sensing image classification has reached a certain bottleneck.

Therefore, in order to effectively improve the accuracy and robustness of remote sensing vegetation resource classification, this work adopts the combination of deep neural network and RS image data for remote sensing vegetation resource classification. The main innovations and contributions of this work include:

(1) Deep neural networks can learn advanced semantic features of remote sensing images, while composite multi-source remote sensing data can provide rich spectral, spatial and temporal information, and the combination of the two can improve the accuracy of vegetation classification.

(2) Different types and stages of vegetation exhibit complex spectral change characteristics. RS data input into the deep network can learn more robust feature representations and improve the adaptability of the model to complex environments.

(3) The local deep neural network is applied to remote sensing image classification, and a new remote sensing image classification algorithm based on local features and deep neural network is proposed. The experimental results show that compared with the traditional DCNN model, the proposed local deep neural network has a better classification effect with higher accuracy and classification efficiency.

## 2. **RS data and its pre-processing.**

### 2.1. **Data storage.**

The adopted RS data storage system is divided into five main layers, including the front-end part, Spring MVC control layer, service implementation layer (service interface layer), persistence layer and database.

The database in the RS data storage system architecture is chosen to be managed by Access 2016. Among them, except for the front-end part, the rest of them can be used as a public service platform to provide API interfaces for other applications and achieve network resource sharing. The project persistence layer is constructed using Mybatis to achieve mapping of the spatial information body and data table of RS data. The commonly used jar package for web applications is used in the Spring MVC control layer [25]. Ajax asynchronous calls were used in the front-end part to visualise the spatial information mainly in the user interface. In order to carry out accurate data matching of the information and number of management subjects in the RS data storage system, a rational design was carried out in terms of multiple attributes. In addition, the association between map subject data and attribute data needs to be constructed in order to perform graphical interaction. The remote sensing image vector information is stored in Access database in Maplnfo standard file format. The association between the graphic file and the attribute data is shown in Figure 1.

### 2.2. **Image pre-processing.**

The remote sensing data sharing platform downloads two remote sensing data separately, including the multiband remote sensing image with the number of bands 7 and the multiband infrared remote sensing image with the number of bands 11 taken by the satellite. The former was captured in August 2017 by Landsat (WorldView2 Tm), which has higher spatial resolution and higher positioning accuracy, and the latter was captured in November 2017 by Landsat (WorldView2 OLI), which has a thermal infrared sensor. In addition, Digital elevation model (DEM) data downloaded from the China Remote Sensing Data Network (CRSDN) [26] with a resolution of $30m \times 30m$ was used.

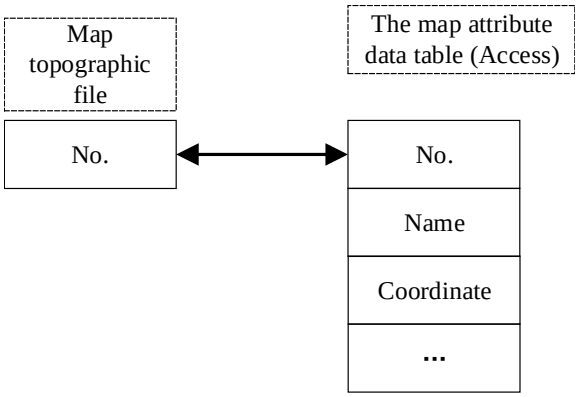


Figure 1. Graphics files associated with attribute data

For the pre-processing of RS data mentioned above, the remote sensing images collected by the two satellites firstly need pre-processing such as radiometric calibration, FLAASH atmospheric correction, band combination and image cropping, and then DEM is used to realise terrain correction. The pre-processed remote sensing image is shown in Figure 2.

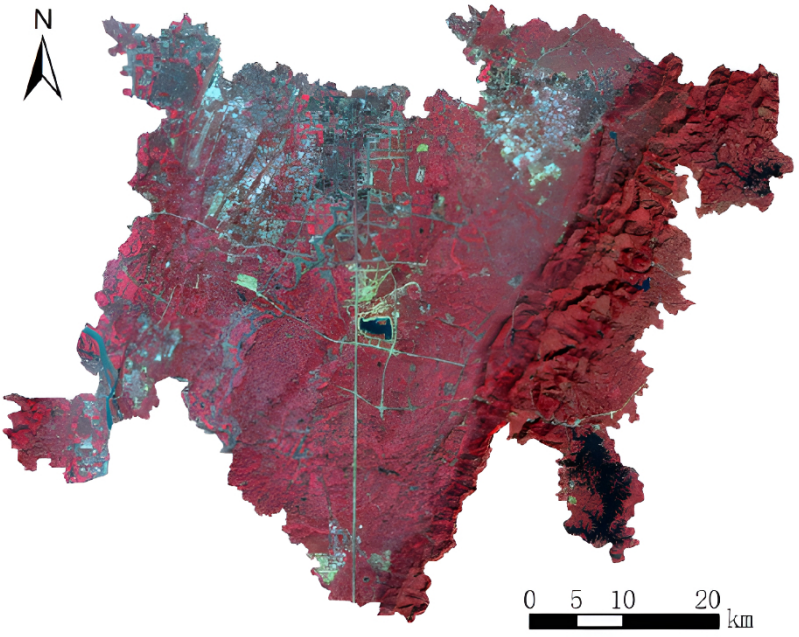


Figure 2. Pre-processed remote sensing images

2.3. **Fusion of RS images.** In general, it is difficult to obtain high-resolution remote sensing image data when carrying out remote sensing vegetation resource classification, which affects the final classification effect to a certain extent. Therefore, after combining RS data preprocessing with GIS technology, in order to improve the accuracy of the subsequent classification of vegetation resources, this paper also uses remote sensing image fusion technology to process remote sensing images.

Specifically, multi-source remote sensing images with the same GIS information are used to fuse the vegetation in a certain area, so as to get the information containing more accurate and rich information. The method uses a variety of remote sensing images with different resolutions and spectral resolutions under the same GIS conditions, which not only enhances the feature information, but also enhances the terrain information.

Feature-level fusion was used. Firstly, radiometric and geometric corrections are applied to the multi-source remote sensing images to achieve the coordinate alignment of each source data. Feature extraction, such as texture features, shape features, colour features, etc., is performed on each remote sensing image. Common feature extraction methods were used, including grey scale covariance matrix, LBP and HOG.

In order to use the fused features for subsequent classification tasks, extraction of relevant attribute data and spatial data was carried out through RS and GIS databases. The format of the 3D model data in the system is OSGB format file. For web presentation in the front-end part, the 3D Tile format file of the 3D model data needs to be converted and loaded [27]. Use Toolbox toolkit in GIS platform to convert relevant vector data into shapefile file format, including selection, zoom in, zoom out, full-screen display, etc. The geographic coordinates of remotely sensed vegetation resources are calculated as follows:

$$\begin{cases} tile_x = |piexl_x \div width| \\ tile_y = |piexl_y \div width| \end{cases} \tag{1}$$

In the formula, *width* denotes the side length of the block, which usually takes the value of 256, $tile_x$ and $tile_y$ denote the horizontal and vertical coordinates of the block, respectively.

Then, each feature is weighted and averaged according to its weight using the weighted average fusion method [28]. The fused feature expression is:

$$F_{\text{usion}} = \sum (w_i \cdot F_i) \tag{2}$$

where $w_i$ is the weight of the $i$-th feature and $F_i$ is the $i$-th feature.

Using Principal Component Analysis (PCA) fusion method, each feature is downscaled to a lower dimension and then the lower dimensional features of different features are fused. The expression of the fused features is:

$$F_{\text{usion}} = \text{PCA}(F_1, F_2, ..., F_n) \tag{3}$$

where $F_1, F_2, ..., F_n$ is the feature vector of different features after PCA dimensionality reduction.

## 3. **Vegetation resource classification based on deep neural network and RS image data.**

3.1. **Local Classifiers.** Local features extracted from different high resolution satellite remote sensing image data using simple windows are called image blocks [29]. The image blocks and local features are processed alternatively. In addition, in our proposed Local DenseNet Neural Network (LDDNN), the main goal is to learn how to classify local features based on image information. Finally, all classification test results are generated by voting method.

In this paper, we set $c = 1, ..., C$ as the classification variable. Assume that each local feature is $\mathbf{x}^{[i]}$, $i = 1, ..., F$. Each local feature contains information that is used for the final classification label of $\mathbf{x}$, so this paper sets the local classification variable to $c_i \in \{1, ..., C\}$.

According to the above formulation, $\mathbf{x}$ belongs to the posterior probability of $c$ and can therefore be derived from the overall model (containing all local feature labels) analysis [30]:

$$p(c|\mathbf{x}) = \sum_{c_1=1}^{C} \cdots \sum_{c_F=1}^{C} p(c, c_1, ..., c_F|\mathbf{x}) \tag{4}$$

In this paper, the model is split into two sub-models, one of which computes the local classification posterior (only $\mathbf{x}$) and the other predicts the full classification posterior.

$$p(c, c_1, ..., c_F|\mathbf{x}) = p(c_1, ..., c_F|\mathbf{x})p(c|\mathbf{x}, c_1, ..., c_F) \tag{5}$$

In order to implement the model, an application-specific model needs to be constructed for $p(c|x)$. In this paper, the first sub-model is simplified by assuming that the local labels are independent of $\mathbf{x}$. The simplification method uses a plain Bayesian decomposition.

$$p(c_1, ..., c_F|\mathbf{x}) = \prod_{i=1}^{F} p(c_i|\mathbf{x}^{[i]}) \tag{6}$$

where $\mathbf{x}^{[i]}$ denotes the portion of $\mathbf{x}$ that is relevant to the prediction $c_i$, such as the i-th image block.

The simplification process assumes the independence of local features. By this simplification method, a relatively simplified model can be obtained. Similarly, the second sub-model also assumes that the overall labels depend only on the local labels, thus achieving the simplification process as follows:

$$p(c|\mathbf{x}, c_1, ..., c_F) := p(c|c_1, ..., c_F) \tag{7}$$

In order to apply this simplified model to practical high-resolution satellite remote sensing image classification scenarios, this paper further optimises the second sub-model by assuming that $\alpha$ denotes the predefined reliable weights (representing the feature information), and using each local feature $i$ to complete the voting on $c_j$:

$$p(c \mid c_1, ..., c_F) = \sum_{i=1}^{F} \alpha_i \delta(c_i, c) \tag{8}$$

where $\delta(\cdot, \cdot)$ is the Kronecker function.

$$p(c \mid \mathbf{x}) = \sum_{i=1}^{F} \alpha_i p(c \mid \mathbf{x}^{[i]}) = \sum_{i=1}^{F} \alpha_i p_c^{[i]} \tag{9}$$

where $p_c^{[i]}$ denotes the predicted probability of the feature $\mathbf{x}^{[i]}$ (relative to the image $\mathbf{x}$ global classification $c$).

A simple weighted average of the a posteriori probabilities of all local classifications $c$ is performed, where each feature still has the predicted weight $\alpha_i$ ( $0 \leq \alpha_i \leq 1, i = 1, ..., F$, and $\sum_i \alpha_i = 1$ ) to generate the final judgement [31]. For simplified analysis, this paper assumes that all local features have the same weight.

$$\alpha_1 = \alpha_2 = \ldots = \alpha_F = \frac{1}{F} \tag{10}$$

In addition, for most $\alpha_i$, it is necessary to set the confidence or resolution of each local feature, or at least some substitution information.

Finally, in this paper, the final classification result of the original image $\mathbf{x}$ is obtained by using the classification with maximum local a posteriori probability weighted sum and ensemble Bayesian decision criterion.

$$\mathbf{x} \to c(\mathbf{x}) = p(c|\mathbf{x}) = \sum_{i=1}^{F} \alpha_i p_c^{[i]} \tag{11}$$

Thus, the overall classification is computed based on the sum of local a posteriori weights for each local feature. Then, the classification with the most votes among all local features is selected as the final classification.

3.2. **Local Classification Posterior Estimation on LDDNN.** The key problem in using local features is that the classification decision boundary has nonlinear and multimodal problems. For such special problems, the local classification posterior needs to be estimated for small image chunks (containing partial information about the image). These small image chunks often give rise to high multimodal distributions.

Therefore, in this paper, nonlinear and multimodal evaluation algorithms, such as the nearest neighbour algorithm, are used to solve such probability distribution problems. The neural network can handle the nonlinear problem. In addition, during the experimental process, the classification posterior estimation is faster and the method can be optimised by matrix operations, thus enabling batch processing. Based on the above claimed problems, this paper proposes to use LDDNN for local classification posterior estimation. In this paper, the deep learning architecture can solve the complex mapping problem between image blocks and classification, as shown in Figure 3.

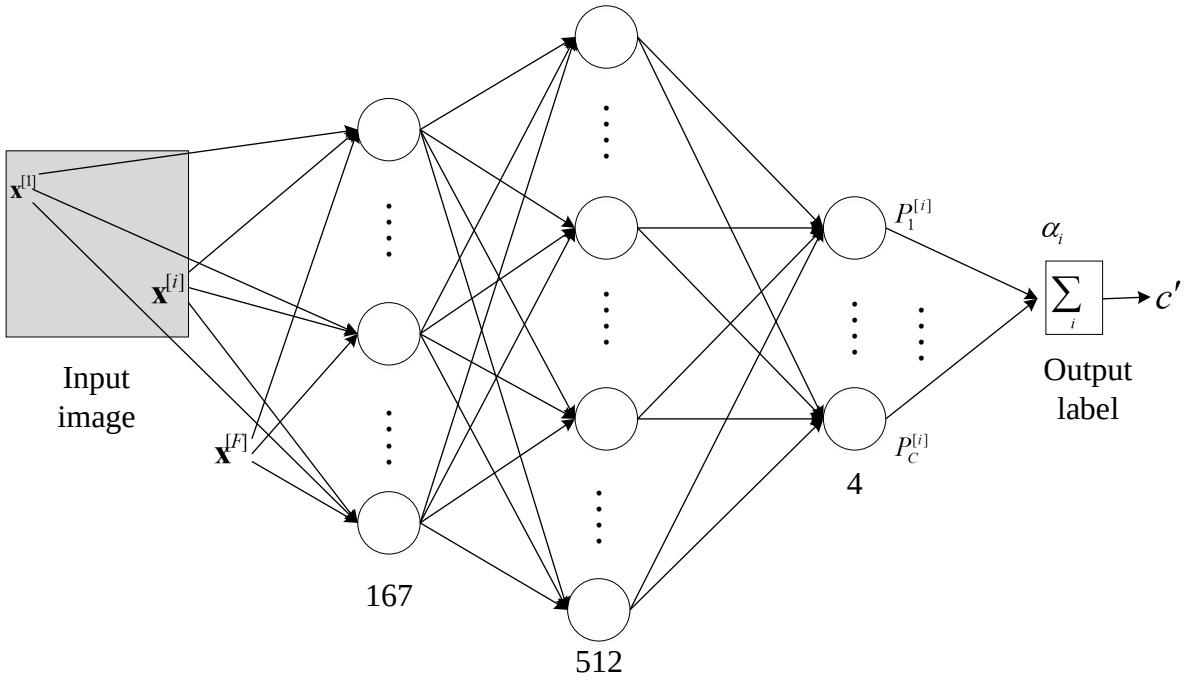


Figure 3. The LDDNN model

It can be seen that in this paper, multiple image blocks are extracted from the original image and these features are fed to a deep neural network used for judgement. The network includes multiple input layers and hidden layers (fully connected). The output layer represents a posteriori probability of each local feature. Finally, a summation operation is performed on all local a posteriori probability. In training, the neural network classifies each image block according to the image label it belongs to. In experiments, in this paper, the classification of all image blocks is processed and then that image is classified according to the final labels.

There are many ways that can be used to define local features of an image, such as size or shape. However, in this paper we only consider square windows of size. For the locations extracted from these image blocks, the simplest method is to use a fixed sampling grid for the input image [32]. However, due to the large number of image blocks, this method results in a large computational cost. Therefore, in this paper, we choose to use some of the image blocks containing high information content and discard the rest of the image blocks with very low relevance.

Following the above method, this paper first obtains a matching binary mask image based on the input image. The centre of each image block to be extracted i.e. effective pixel. Deep learning uses a pre-trained LDDNN as a feature extractor and adds a fully connected layer on top of it for classification. A cross-entropy loss function is used for the classification task and a stochastic gradient descent (SGD) optimiser is used for parameter optimisation.

3.3. **Methodology for the classification of remotely sensed vegetation resources.** This work uses the Keras library to build and train a remote sensing image classification method based on LDDNN model and RS image data. First, the desired library is imported and the RS data is preprocessed to extract relevant attribute data and spatial data, thus forming the initial input image. Then, the DenseNet model is constructed and the global average pooling layer and fully connected layer are added. Next, the DenseNet underlying weights are frozen in order to remain constant during training. Finally, the model is compiled and trained using the training data. Observe the process of Loss vs. Accuracy, evaluate the performance of the model on the validation data, and make adjustments to the parameters in order to obtain higher accuracy.

The forward propagation in the LDDNN model is shown below:

$$\mathbf{y} = f_c(f_{gp}(f_{db}(f_{conv}(x)))) \tag{12}$$

where $x$ is the initial input image data after preprocessing, $f_{conv}$ is the convolutional layer, $f_{db}$ is the DenseBlock, $f_{gp}$ is the global average pooling layer, and $f_c$ is the fully connected layer, and $\mathbf{y}$ is the output classification result.

The loss function is calculated as shown below:

$$L = -\frac{1}{N}\sum_{i=1}^{N}\sum_{j=1}^{C} y_{ij}\log(\hat{y}_{ij}) \tag{13}$$

where $N$ is the number of samples, $C$ is the number of categories, $y_{ij}$ is the true label of the $i$-th sample, and $\hat{y}_{ij}$ is the predicted label of the $i$-th sample.

The SGD optimiser for the LDDNN model is:

$$\theta_{t+1} = \theta_t - \alpha\nabla L(\theta_t) \tag{14}$$

where $\theta_t$ is the model parameter at the t-th iteration, $\alpha$ is the learning rate, and $\nabla L(\theta_t)$ is the gradient of the loss function $L$ with respect to the model parameter $\theta_t$.

The LDDNN-RS based remote sensing vegetation resource classification method is shown in Algorithm 1.

**Algorithm 1** LDDNN-RS based remote sensing vegetation resource classification

```
# Import the required libraries
import os
import numpy as np
from keras.preprocessing.image import ImageDataGenerator
from keras.applications import DenseNet121
from keras.layers import Dense, GlobalAveragePooling2D
from keras.models import Model
from keras.optimizers import Adam
# Data pre-processing
train datagen = ImageDataGenerator(rescale=1./255)
test datagen = ImageDataGenerator(rescale=1./255)
train generator = train datagen.flow from directory(
    train data dir,
    target size=(img height, img width),
    batch size=batch size,
    class mode='categorical')
validation generator = test datagen.flow from directory(
    validation data dir.
    target size=(img height, img width),
    batch size=batch size,
    class mode='categorical')
# Constructing the DenseNet model
base model = DenseNet121(weights='imagenet', include top=False)
x = base model.output
x = GlobalAveragePooling2D()(x)
predictions = Dense(num classes, activation='softmax')(x)
model = Model(inputs=base_model.input, outputs=predictions)
# Freeze DenseNet underlying weights
for layer in base model.layers:
    layer.trainable = False
# Compile the model
model.compile(optimizer=Adam(lr=0.001), loss='categorical crossentropy', metrics=['accuracy'])
# Training models
model.fit generator(
    train generator.
    steps per epoch=num train samples // batch size,
    epochs=epochs,
    validation data=validation generator,
    validation steps=num validation samples // batch size)
# Evaluating models
score=model.evaluate generator(validation generator, num validation samples : batch size)
print('Test loss:', score[0])
print('Test accuracy:', score[1])
```

## 4. **Experimental results and analyses.**

4.1. **Experimental environment.** The operating environment for the experiments in this work is divided into 2 main parts: the hardware environment and the software environment, the specific parameters are shown in Table 1. Classification tests for remote sensing

Table 1. Parameters of the environment in which the experiment will be run

| operating environment | parametric | numerical value |
|---|---|---|
| hardware environment | CPU | Intel i5 9600KF@3.7GHz |
| | hard drive | 200GB |
| | random access memory (RAM) | 4GB |
| | Graphic image processing equipment | GTX1050@2GB GDDR5 |
| software environment | OS system | Windows 10 |
| | development platform (computing) | 3DMAX, ENVI, GIS, Python |
| | comprehensive database | Access |

vegetation resource classification were conducted using DCNN [23]-RS and LDDNN-RS, respectively, and the classification efficiency and accuracy of the three methods were compared. The LDDNN proposed in this paper requires fewer parameters to be set, the size of the image block is 13×13 pixels, the hidden layer has 512 Rectified linear unit (ReLU) and the input layer has 4 units.

4.2. **WorldView2 satellite remote sensing image data.** WorldView2 high resolution satellite remote sensing images were used for the experiments in this work, and the WorldView2 parameters are shown in Table 2. The dataset is divided into a training set of 1500 sheets and a validation set of 645 sheets according to the ratio of 7:3. The training set is used to train the model, and the validation set is used to adjust the hyperparameters and evaluate the model performance during the training process. Each image in the Panchromatic Band (PB) dataset contains 3 channels, the image format is an 8-bit TIFF file, and the value domain of image elements is [0,255]. Each image in the Multispectral Band (MB) dataset contains 6 channels, the image format is a 16-bit TIFF file, and the value domain of the image element is [0,65535].

Table 2. Parameters of WorldView2

| Transducers | Spatial resolution/m | Wavelength/nm |
|---|---|---|
| Panchromatic band (PB) | 0.5 | 450-1040 |
| | | 400-450 |
| | | 450- 510 |
| Multi-spectral band (MB) | 1.8 | 510-580 |
| | | 585-625 |
| | | 630-690 |
| | | 705-745 |
| | | 770-895 |
| | | 860-1040 |

As shown in Table 3, all the image elements in the dataset are classified with labels, of which 31.2 % are labelled as bare ground, 42.1 % are labelled as vegetation, and 20.6 % are labelled as water. Another 5.9 % of the image elements are labelled as unclassified and are ignored during model training and validation. In order to increase the generalisation ability of the model during the training process, each image is randomly rotated, as well as a certain degree of uniform random brightness adjustment for all bands, before entering the model training.

Table 3. Category proportion

| No. | Category | Percentage % |
|---|---|---|
| 0 | bare ground | 31.2 |
| 1 | plant cover | 42.1 |
| 2 | (of clothes) classifier for number of washes | 20.6 |
| 3 | Uncategorised | 5.9 |

4.3. **Remote sensing vegetation resource classification results.** Spectral images and high-resolution single-band images are fused into a single image. The bilinear interpolation resampling method was chosen to obtain the best visual effect and information extraction capability.

Using the Gram-Schmidt spectra sharpening tool in the ENVI software, multiple low-resolution multiluminous were used to prevent network overfitting using an Early Stopping strategy, i.e., training was stopped when the metrics no longer improved or began to decline. The trained network models were evaluated for performance using the validation set in each dataset, and the confusion matrix was used to calculate and count the accuracy. The confusion matrix metrics were used to quantitatively assess the classification accuracy from four aspects, and the final results of the remote sensing vegetation resource classification accuracy are shown in Table 4.

Table 4

| Assessment of indicators | Value % |
|---|---|
| error in grading | 6.48 |
| missmissing fraction error | 2.90 |
| Overall classification accuracy | 91.66 |
| Kappa factor | 90.35 |

It can be seen that after the pre-processing of composite remote sensing data and fusion of remote sensing images, the overall classification accuracy and Kappa coefficient of the maximum likelihood classification results of vegetation resources are higher than 90%, which meets the requirements of practical applications.

4.4. **Comparison of classification performance.** The comparison between the classification prediction results of the DCNN-RS model and the LDDNN-RS model is shown in Figure 4, where yellow indicates bare land classification, green indicates vegetation classification, and blue indicates water body classification.

It can be clearly seen that the PB image is rougher in the edge profile in the classification results on the DCNN-RS model. Whereas, MB image performs better on the same DCNN-RS model and is more accurate in predicting the classification of geomorphic edges. For the DCNN-RS model, MB improves the overall classification accuracy by 11.83 % over PB on training

In addition, for the MB image dataset, the LDDNN-RS model proposed in this paper is compared with the DCNN-RS model and the DCNN model, and the results of the classification accuracy as well as the classification usage time are shown in Table 5. From Table 5, it can be seen that compared with the DCNN-RS model, the classification time of the LDDNN-RS model proposed in this paper is slightly longer, but the average classification accuracy is improved by 11.16%, which is due to the fact that, the nearest-neighbour algorithm estimation in the LDDNN-RS model needs to analyse all the extracted local

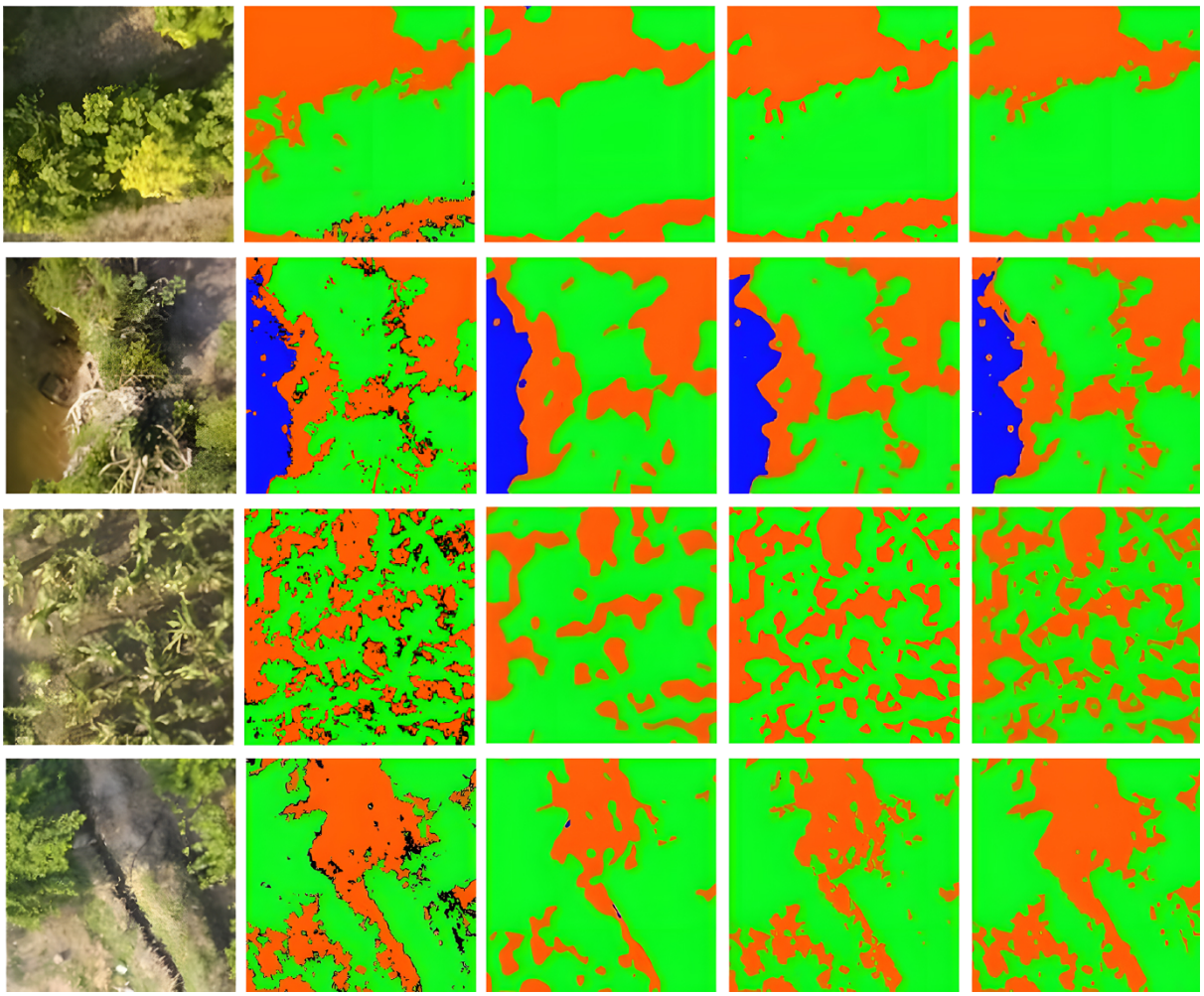

Figure 4. Classification results Results. (a) original image; (b) real labels; (c) PB+DCNN-RS; (d) MB+DCNN-RS; (e) MB+LDDNN-RS

features, which is a more computationally intensive process. Compared with the traditional DCNN model, the average classification time of the LDDNN-RS model is reduced by 1307.7s and the average classification accuracy is improved by 3.48%.

In summary, compared with the existing DCNN models, the LDDNN-RS model proposed in this paper obtains higher classification accuracy and classification efficiency by local feature extraction first and then deep learning based on these features.

5. **Conclusion.** The author proposed a classification method for vegetation resources based on deep neural network and composite remote sensing image data. Using RS image data, the relevant attribute data and spatial data of vegetation resources are extracted to form a preliminary input image. From the initial input image, a variety of local characteristics are retrieved and fed to a deep neural network for evaluation. The assigned picture labels are used to categorize each local feature. Judge the overall image based on a simple voting method. The experimental results on WorldView2 show that compared to the DCNN-RS model, the classification time of the LDDNN-RS model is slightly longer, but the average classification accuracy is improved by 11.16%; compared to the traditional DCNN model, the average classification time of the LDDNN-RS model is reduced by 1307.7s, and the average classification accuracy is improved by 3.48%. From the perspective of deep learning models, more excellent semantic segmentation models

Table 5. Comparisons of results from three classification methods

| Classification | Number of classifications | Accuracy/per cent | Time/s |
|---|---|---|---|
| DCNN | 1 | 88.65 | 1673.76 |
| | 2 | 88.68 | 1678.45 |
| | 3 | 89.12 | 1685.61 |
| | 4 | 86.32 | 1697.62 |
| | 5 | 88.12 | 1685.92 |
| | average value | 88.18 | 1684.27 |
| DCNN-RS | 1 | 81.57 | 297.22 |
| | 2 | 81.06 | 301.13 |
| | 3 | 79.51 | 308.92 |
| | 4 | 79.32 | 306.82 |
| | 5 | 81.07 | 299.56 |
| | average value | 80.51 | 302.73 |
| LDDNN-RS | 1 | 91.72 | 381.95 |
| | 2 | 91.78 | 361.07 |
| | 3 | 92.21 | 384.63 |
| | 4 | 91.02 | 374.42 |
| | 5 | 91.58 | 381.03 |
| | average value | 91.66 | 376.62 |

have appeared in the field of image segmentation in recent years, such as Segment and Deeplabv3. Therefore, the subsequent research will try to use more advanced semantic segmentation models as the benchmark models to further improve the classification accuracy.

## REFERENCES

[1] Y. Ma, Y. Peng, and T.-Y. Wu, "Transfer learning model for false positive reduction in lymph node detection via sparse coding and deep learning," *Journal of Intelligent & Fuzzy Systems*, vol. 43, no. 2, pp. 2121-2133, 2022.

[2] F. Zhang, T.-Y. Wu, J.-S. Pan, G. Ding, and Z. Li, "Human motion recognition based on SVM in VR art media interaction environment," *Human-centric Computing and Information Sciences*, vol. 9, 40, 2019.

[3] F. Zhang, T.-Y. Wu, and G. Zheng, "Video salient region detection model based on wavelet transform and feature comparison," *EURASIP Journal on Image and Video Processing*, vol. 2019, 58, 2019.

[4] M. Zhao, Y. Zhou, X. Li, W. Cao, C. He, B. Yu, X. Li, C. D. Elvidge, W. Cheng, and C. Zhou, "Applications of satellite remote sensing of nighttime light observations: Advances, challenges, and perspectives," *Remote Sensing*, vol. 11, no. 17, 1971, 2019.

[5] A. L. H. P. Shaik, M. K. Manoharan, A. K. Pani, R. R. Avala, and C.-M. Chen, "Gaussian Mutation–Spider Monkey Optimization (GM-SMO) Model for Remote Sensing Scene Classification," *Remote Sensing*, vol. 14, no. 24, pp. 6279, 2022.

[6] E. K. Wang, C.-M. Chen, M. M. Hassan, and A. Almogren, "A deep learning based medical image segmentation technique in Internet-of-Medical-Things domain," *Future Generation Computer Systems*, vol. 108, pp. 135-144, 2020.

[7] K.-K. Tseng, R. Zhang, C.-M. Chen, and M. M. Hassan, "DNetUnet: a semi-supervised CNN of medical image segmentation for super-computing AI service," *The Journal of Supercomputing*, vol. 77, no. 4, pp. 3594-3615, 2020.

[8] G. Meraj, S. Kanga, A. Ambadkar, P. Kumar, S. K. Singh, M. Farooq, B. A. Johnson, A. Rai, and N. Sahu, "Assessing the yield of wheat using satellite remote sensing-based machine learning algorithms and simulation modeling," *Remote Sensing*, vol.

14, no. 13, 3005, 2022.
[9] Z. Shao, W. Wu, and D. Li, "Spatio-temporal-spectral observation model for urban remote sensing," *Geo-Spatial Information Science*, vol. 24, no. 3, pp. 372-386, 2021.
[10] S. Prakash, and H. Norouzi, "Land surface temperature variability across India: a remote sensing satellite perspective," *Theoretical and Applied Climatology*, vol. 139, pp. 773-784, 2020.
[11] S. Fabbrocino, E. Bellucci Sessa, S. de Vita, M. A. Di Vito, R. Avino, and E. Marotta, "A GIS-Based Hydrogeological Approach to the Assessment of the Groundwater Circulation in the Ischia Volcanic Island (Italy)," *Frontiers in Earth Science*, vol. 10, 883719, 2022.
[12] M. El Garouani, M. Amyay, A. Lahrach, and H. J. Oulidi, "Land surface temperature in response to land use/cover change based on remote sensing data and GIS techniques: Application to Saïss Plain, Morocco," *Journal of Ecological Engineering*, vol. 22, no. 7, pp. 100-112, 2021.
[13] M. Weiss, F. Jacob, and G. Duveiller, "Remote sensing for agricultural applications: A meta-review," *Remote Sensing of Environment*, vol. 236, 111402, 2020.
[14] L. Zhang, and L. Zhang, "Artificial intelligence for remote sensing data analysis: A review of challenges and opportunities," *IEEE Geoscience and Remote Sensing Magazine*, vol. 10, no. 2, pp. 270-294, 2022.
[15] L. Congedo, "Semi-Automatic Classification Plugin: A Python tool for the download and processing of remote sensing images in QGIS," *Journal of Open Source Software*, vol. 6, no. 64, 3172, 2021.
[16] L. Ma, Y. Liu, X. Zhang, Y. Ye, G. Yin, and B. A. Johnson, "Deep learning in remote sensing applications: A meta-analysis and review," *ISPRS Journal of Photogrammetry and Remote Sensing*, vol. 152, pp. 166-177, 2019.
[17] Q. Yuan, H. Shen, T. Li, Z. Li, S. Li, Y. Jiang, H. Xu, W. Tan, Q. Yang, and J. Wang, "Deep learning in environmental remote sensing: Achievements and challenges," *Remote Sensing of Environment*, vol. 241, 111716, 2020.
[18] W. Zhang, H. Li, Y. Li, H. Liu, Y. Chen, and X. Ding, "Application of deep learning algorithms in geotechnical engineering: a short critical review," *Artificial Intelligence Review*, vol. 11, pp. 1-41, 2021.
[19] T. Wang, M. M. Crawford, and M. R. Tuinstra, "A novel transfer learning framework for sorghum biomass prediction using UAV-based remote sensing data and genetic markers," *Frontiers in Plant Science*, vol. 14, 1138479, 2023.
[20] X.-X. Zhou, Y.-Y. Li, Y.-K. Luo, Y.-W. Sun, Y.-J. Su, C.-W. Tan, and Y.-J. Liu, "Research on remote sensing classification of fruit trees based on Sentinel-2 multi-temporal imageries," *Scientific Reports*, vol. 12, no. 1, 11549, 2022.
[21] L. Zhao, Q. Li, Y. Zhang, H. Wang, and X. Du, "Integrating the continuous Wavelet transform and a convolutional neural network to identify Vineyard Using Time series satellite images," *Remote Sensing*, vol. 11, no. 22, 2641, 2019.
[22] Y. Guo, and H. Ren, "Remote sensing monitoring of maize and paddy rice planting area using GF-6 WFV red edge features," *Computers and Electronics in Agriculture*, vol. 207, 107714, 2023.
[23] S. Shao, R. Yan, Y. Lu, P. Wang, and R. X. Gao, "DCNN-based multi-signal induction motor fault diagnosis," *IEEE Transactions on Instrumentation and Measurement*, vol. 69, no. 6, pp. 2658-2669, 2019.
[24] H. Kim, "Feasibility of DRNN for Identifying Built Environment Barriers to Walkability Using Wearable Sensor Data from Pedestrians' Gait," *Applied Sciences*, vol. 12, no. 9, 4384, 2022.
[25] Y. Febrianes, and P. O. N. Saian, "Pembangunan Aplikasi Permintaan Cuti Berbasis Web Menggunakan Framework Hibernate dan Spring MVC," *Journal of Applied Computer Science and Technology*, vol. 2, no. 1, pp. 33-42, 2021.
[26] N. Saleem, M. E. Huq, N. Y. D. Twumasi, A. Javed, and A. Sajjad, "Parameters derived from and/or used with digital elevation models (DEMs) for landslide susceptibility mapping and landslide risk assessment: a review," *ISPRS International Journal of Geo-Information*, vol. 8, no. 12, 545, 2019.
[27] D. Furcy, S. M. Summers, and L. Withers, "Improved lower and upper bounds on the tile complexity of uniquely self-assembling a thin rectangle non-cooperatively in 3d," *Theory of Computing Systems*, pp. 1-49, 2023.
[28] Y. Liu, L. Wang, J. Cheng, C. Li, and X. Chen, "Multi-focus image fusion: A survey of the state of the art," *Information Fusion*, vol. 64, pp. 71-91, 2020.
[29] S.-H. Wang, and Y.-D. Zhang, "DenseNet-201-based deep neural network with composite learning factor and precomputation for multiple sclerosis classification," *ACM Transactions on Multimedia Computing, Communications, and Applications (TOMM)*, vol. 16, no. 2s, pp. 1-19, 2020.

[30] J. Hemalatha, S. A. Roseline, S. Geetha, S. Kadry, and R. Damaševičius, "An efficient densenet-based deep learning model for malware detection," *Entropy*, vol. 23, no. 3, 344, 2021.
[31] S. Zhai, D. Shang, S. Wang, and S. Dong, "DF-SSD: An improved SSD object detection algorithm based on DenseNet and feature fusion," *IEEE Access*, vol. 8, pp. 24344-24357, 2020.
[32] W. Tong, W. Chen, W. Han, X. Li, and L. Wang, "Channel-attention-based DenseNet network for remote sensing image scene classification," *IEEE Journal of Selected Topics in Applied Earth Observations and Remote Sensing*, vol. 13, pp. 4121-4132, 2020.